Real-time plug-in electric vehicle charging strategies for current and voltage unbalance minimization

Julian A. Fernandez [1], **Delphine Riu** [2], **Seddik Bacha** [2], **Marc Paupert** [3], **Ahmad Hably** [1]

1. *GIPSA-Lab Grenoble Images Parole Signal Automatique Laboratoire, University of Grenoble Alpes, 11 rue des Mathématiques, BP46, 38402 Saint Martin D'Hères, France*
   fernandjul@gmail.com/ahmad.hably@gipsa-lab.grenoble-inp.fr
2. *G2ELab Grenoble Electrical Engineering Laboratory, University of Grenoble Alpes, France*
   delphine.riu@g2elab.grenoble-inp.fr
3. *Schneider Electric R&D, 31 rue Pierre Mendes France, 38320 EYBENS, France*
   marc.paupert@schneider-electric.com

ABSTRACT. *Plug-in electric vehicles (PEVs) have been proposed as one of the solutions to reduce transportation dependency on oil. Nevertheless, if PEVs are introduced as a new load on the grid without any charging strategy, the grid's power quality will be deteriorated. Among the power quality parameters, current and voltage unbalances would be affected. This paper proposes a real-time strategy in order to minimize the current unbalance factor (CUF) caused by PEVs and housing on a common connection point (CCP) in a residential network. As a consequence of the CUF minimization, the voltage unbalance factor (VUF) is significantly reduced. The CUF at a CCP is formulated as a function of the loads in-phase and quadrature currents (PEVs and householders included). This objective function is minimized under maximum rating and charging priority constraints using algorithm Active-set. The minimization process is a part of the strategy which consists in adapting the optimization problem in real-time to changing conditions such as PEV's arrival and departure times, PEV's battery capacity variety, a random initial state-of-charge (SOC) and the householder's consumption. The strategy was tested on a low voltage network simulated on Matlab®/Simulink®. Results show that the current balance index is increased more than 400%, the voltage unbalance index is reduced 17% and some of the CCPs in the electric network simulated, are re-balanced (based on the EN50160 standard's definition) thanks to the CUF minimization.*

RÉSUMÉ. *Les véhicules électriques rechargeables (Plug-in electric vehicles - PEV) ont été proposés comme une des solutions pour réduire la dépendance du transport par rapport au pétrole.*

Journal européen des systèmes automatisés – n° 3/2016, 271-298

Malgré ceci, si les PEV s'envisagent comme une nouvelle charge du réseau sans aucune gestion, la qualité d'énergie sera dégradée. Parmi les paramètres caractérisant la qualité d'énergie, le déséquilibre triphasé en courant et en tension seront impactés de façon importante. Cet article propose une stratégie en temps réel qui cherche à minimiser le taux de déséquilibre triphasé en courant (Current Unbalance Factor - CUF) celui-ci étant une conséquence de la consommation des PEV et des lotissements au niveau de points de connexion commun (Common Connection Points - CCP) dans un réseau résidentiel. En plus, le taux de déséquilibre triphasé en tension (Voltage Unbalance Factor - VUF) est réduit par l'effet de la minimisation du CUF. Le CUF a été formulé en fonction des courants en-phase et en-quadrature des charges (PEV et Lotissements d'usagers inclus). Cette fonction objective a été minimisée en tenant compte des restrictions liées aux usagers et aux PEV telles que la puissance maximale de charge/décharge et état de charge (State-of-Charge - SOC) maximale au moment du départ. L'algorithme Active-Set a été utilisé pour résoudre le problème d'optimisation. De plus, la stratégie de minimisation du CUF consiste à adapter les paramètres d'entrée à l'algorithme d'optimisation en temps réel en adaptant la réponse de l'optimisateur aux changements des conditions du CCP choisi (arrivée au départ des PEV, SOC initial aléatoire, consommation des usagers). La stratégie a été simulée dans un modèle de réseau de basse tension sur MatLab®/Simulink®. Les résultats montrent que l'index de l'équilibre en courant est augmenté plus de 400% et l'index de déséquilibre en tension est réduit jusqu'à 17% ; en plus, plusieurs CCP ont été rééquilibrés (en se basant dans la norme EN50160) grâce à la minimisation du CUF.

KEYWORDS: *Electric vehicle integration, V2G, current unbalance, voltage unbalance, smartgrid, convex optimization*

MOTS-CLÉS : *Intégration de véhicules électriques rechargeables, V2G, Déséquilibre triphasé en courant, Déséquilibre triphasé en tension, réseaux intelligents*

DOI:10.3166/JESA.49.271-298

1. Introduction

Impacts of the plug-in electric vehicle (PEV) on the distribution network have been studied extensively (Lassila *et al*., 2012; Turker, Bacha *et al*., 2012a; Gomez, Morcos, 2003). A high penetration of PEVs in the transportation market in addition to the simultaneous usage of charging stations in a low voltage (LV) network (Francfort, 2013) will increase the peak load, activating polluting sources, the aging rate of distribution LV transformers, and in general it will deteriorate the power quality of the grid. A low power quality leads to a less efficient distribution system and consequently, it reduces the sustainability of the whole power system.

Voltage and current unbalances will be considerably affected by the increasing number of single phase charging events in the LV network. In (Shahnia, Ghosh *et al*., 2013), the Impact of the electric vehicle charging on the voltage unbalance is illustrated by simulating several scenarios while varying the charging event location, the market penetration ratio and the charging power level. In (Duvall *et al*., 2011), the

impact of the EV charging on the secondary of a MV/LV transformer is evaluated as a function of the number of EVs connected to the grid.

The authors in (Jayatunga *et al*., 2012) show that one of the main causes of voltage unbalance is the current unbalance at a three-phase common connection point (CCP). Furthermore, current unbalance is a consequence of the load unbalance between the three phases, and such load unbalance will be importantly affected by a high penetration of PEV loads and the variable number of PEVs connected at any moment, the random connection and disconnection times, the variety of battery capacities depending on the PEV's brand, etc.

At the same time, as presented by (Kempton, Letendre, 1997) for the first time, the storage characteristics of PEVs could create an added value for the electric network. This distributed energy storage systems (ESS) would improve the regulation (Sortomme, El-Sharkawi, 2012) as well as it would be essential for the attenuation of renewable energies intermittence (Hu *et al*., 2013) and peak-shaving (Wang, Wang, 2013). The concept of using the PEVs as a distributed resource -load and generation/storage device- by their integration in to the grid is known as vehicle-to-grid (V2G). A review on the actual state of the research on this topic and its future is discussed in (Tuttle, Baldick, 2012).

In this paper, a new V2G application is proposed. A real-time semi-distributed PEV charging strategy is developed for current unbalance minimization under maximum charging current and maximum SOC at departure constraints. The strategy is semi-distributed because the controller is located at the three-phase CCP where the power is delivered to single phase loads which is less distributed than end-user based strategies and less centralized than strategies managing PEVs from the substation level. Such controller will use current and voltage measurements at the CCP as well as information on the availability of each PEV connected for V2G interactions. The connection and disconnection times as well as the priority of a high SOC when leaving the house will determine the availability for V2G as stated by (Mohamed *et al*., 2014). The strategy will deliver optimal active and reactive power set-points (P, Q) for each PEV connected at the CCP in real-time, depending on the time intervals simulated.

Several solutions for current unbalance reduction have been proposed. In (Shahnia *et al*., 2012), the authors have proposed the reduction of the current unbalance in a medium-voltage distribution network by using single-phase distributed photovoltaic production. Each PV converter is controlled to work as a varying capacitor in order to compensate the uncontrollable loads. In (Shahnia, Wolfs, Ghosh, 2013), the authors have proposed a strategy to control the residential loading in order to reduce the voltage unbalance. The ruled-based algorithm proposed controls from the feeder a static transfer switch located at CCP connecting end-users residences, that will transfer the residential loads between phases. A rule-based algorithm coordinating PEVs charging for CU reduction has been proposed in (Fernandez *et al*., 2013). The main objective of the algorithm proposed was to cancel out the negative sequence by using only reac-

tive power delivered from the PEV charger, in order to preserve the battery charging process.

In (Fernandez, Bacha *et al*., 2015) and (Fernandez, Hably, Bratcu, 2015) several optimization methods have been applied to minimize the CUF. In (Fernandez, Bacha *et al*., 2015) the CUF has been formulated as a combinatorial problem where the decision variables are connection/disconnection signals sent to the PEVs. An Ants Algorithm Optimization method has been used to reach a fast (compared to an exhaustive-search method) a good solution (configuration of PEVs connected) for a minimal CUF, given a scenario where the number of PEV owners at the Low Voltage Network is relatively high. In (Fernandez, Hably, Bratcu, 2015), Some results of applying the real-time CUF minimization strategy while adding a positive profit constraint for the PEV owners are presented. By adding this constraint, authors showed under which scenarios, the CUF minimization strategy would represent an interesting business model for both PEV owners and the distribution network operator.

In this paper, the CUF is addressed in detail as an optimization problem whose objective function is given by the current unbalance factor and is minimized using the sequential quadratic programming method under constraints. Moreover, it is illustrated that the voltage unbalance is reduced as consequence of the current unbalance minimization. It will be shown that the effect is different depending on the characteristics of the CCP.

The paper is organized as follows: in Section II, the current unbalance factor is formulated as a function of local PEV variables. Then in Section III, the optimization problem is described. In Section IV, the real-time minimization strategy is presented. The simulation environment is illustrated in Section V. The data collected from the simulation is analyzed in Section VI. In Section VII finally, conclusions and future work are proposed.

2. Current Unbalance Problem formulation

According to the European standard EN50160 (Markiewicz, Klajn, 2004), a three-phase CCP like the one in Fig.1 is unbalanced if 95 % of the time during one week, the measures of the voltage unbalance factor (VUF) are above 0.02. The VUF is defined as:

$$VUF = \left| \frac{\mathbf{V}_2}{\mathbf{V}_1} \right| \tag{1}$$

In eq.(1), $\mathbf{V}_2$ and $\mathbf{V}_1$ represent the negative and the positive sequence voltages respectively, both calculated using the three phase-to-neutral voltages at a CCP. A VUF measure is an average over 10 minutes of the VUF sampled every 30 seconds.

In addition, according to the standard IEEE 1159-2009 (“IEEE Recommended Practice for Monitoring Electric Power Quality”, 2009), the samples of the current

unbalance factor (CUF) in a three-phase CCP has to be below 30% in steady state. The CUF is defined as:

$$CUF = \left| \frac{\mathbf{I}_2}{\mathbf{I}_1} \right| \tag{2}$$

Similar to the VUF, $\mathbf{I}_2$ and $\mathbf{I}_1$ represent the negative and the positive sequence currents respectively, both calculated using the line currents at a CCP. A CUF measure is an average over 10 minutes of the CUF sampled every 30 seconds.

2.1. Relation between the CUF and the PEVs currents

In this section, the relation between the CUF and the in-phase and quadrature load currents is presented. Fig.1 illustrates a common scenario of a LV network feeding a CCP that gathers residential loads including PEVs. It is a three-phase three-wire system with single-phase phase-to-neutral loads with $\mathbf{I}_a$, $\mathbf{I}_b$ and $\mathbf{I}_c$ as the line currents. Each phase-to-neutral voltages is represented by $\mathbf{V}_{aN}$, $\mathbf{V}_{bN}$ and $\mathbf{V}_{cN}$ respectively.

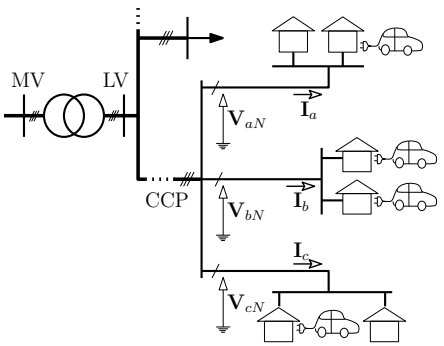

Figure 1. Common connection point (CCP) in a LV network

Assuming the network at its sinusoidal steady state, line currents are the linear combination of their in-phase (identified with the index 'd') and quadrature (identified with the index 'q') components as represented in eq.(3) (Fernandez *et al*., 2013) and as illustrated on Fig.2. The unitary vectors $\mathbf{u}_{x_d}$ and $\mathbf{u}_{x_q}$ are the normalized images of the in-phase and quadrature components of the phase-to-neutral voltages.

$$\begin{aligned} \mathbf{I}_a &= I_{a_d} \cdot \mathbf{u}_{a_d} + I_{a_q} \cdot \mathbf{u}_{a_q} \\ \mathbf{I}_b &= I_{b_d} \cdot \mathbf{u}_{b_d} + I_{b_q} \cdot \mathbf{u}_{b_q} \\ \mathbf{I}_c &= I_{c_d} \cdot \mathbf{u}_{c_d} + I_{c_q} \cdot \mathbf{u}_{c_q} \end{aligned} \tag{3}$$

According to Fortescue, symmetrical sequence currents are defined as follows:

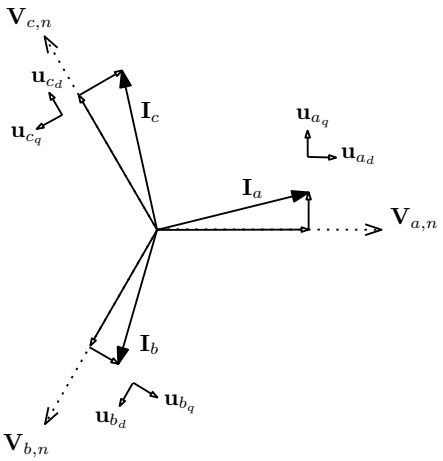

Figure 2. Phasors representation of currents and voltages at the CCP

$$\begin{pmatrix}\mathbf{I}_1\\ \mathbf{I}_2\\ \mathbf{I}_0\end{pmatrix} = \left(\frac{1}{3}\right)\mathbf{F}^{-1}\begin{pmatrix}\mathbf{I}_a\\ \mathbf{I}_b\\ \mathbf{I}_c\end{pmatrix} \tag{4}$$

where $F = \begin{pmatrix}1 & 1 & 1\\ \mathbf{a}^2 & \mathbf{a} & 1\\ \mathbf{a} & \mathbf{a}^2 & 1\end{pmatrix}$ with $\mathbf{a} = e^{2\pi i/3}$.

Thus replacing eq.(3) in eq.(4), a relation between the symmetric components and the in-phase and quadrature components is established. This relation is formulated in eq.(5) taking into account that $\mathbf{u}_{k_q} = \mathbf{u}_{k_d} \cdot e^{-i\pi/2}$ for $k = a, b, c$.

$$\begin{pmatrix}\mathbf{I}_1\\ \mathbf{I}_2\\ \mathbf{I}_0\end{pmatrix} = \left(\frac{1}{3}\right)\begin{pmatrix}1 & 1 & 1\\ 1 & \mathbf{a} & \mathbf{a}^2\\ 1 & \mathbf{a}^2 & \mathbf{a}\end{pmatrix}\begin{pmatrix}\mathbf{u}_{a_d} & 1 & 1\\ 1 & \mathbf{u}_{b_d} & 1\\ 1 & 1 & \mathbf{u}_{c_d}\end{pmatrix} * \left\{\begin{pmatrix}\mathbf{I}_{a_d}\\ \mathbf{I}_{b_d}\\ \mathbf{I}_{c_d}\end{pmatrix} + e^{-i\pi/2}\begin{pmatrix}\mathbf{I}_{a_q}\\ \mathbf{I}_{b_q}\\ \mathbf{I}_{c_q}\end{pmatrix}\right\}$$

In order to simplify the problem and keep the symmetric sequences independent from loads connected to other CCP's, the in-phase unitary vectors will be fixed to the values at perfect balanced voltage conditions as presented in eq.(5). The error produced by this approximation is described later.

$$u_{a_d} = 1, \quad u_{b_d} = e^{2\pi i/3} \quad \text{and} \quad u_{c_d} = e^{4\pi i/3} \tag{5}$$

On the other hand, each line current is the summation of the currents of the loads connected to the corresponding phase. Therefore equations in eq.(3) can be rewritten

as in eq.(6) where x_{d_j} and x_{q_j} are the in-phase and quadrature currents of the j-th PEV out of a group of PEVs. If the j-th PEV is connected to the line a, the j-th PEV belongs to the group C_a ($j \in C_a$) of PEVs. If the j-th PEV is connected to the line b, the j-th PEV belongs to the group C_b ($j \in C_b$) of PEVs. And finally, If the j-th PEV is connected to the line c, the j-th PEV belongs to the group C_c ($j \in C_c$) of PEVs. $I^H_{a_d}$, $I^H_{b_d}$ and $I^H_{c_d}$ are the summation of all the in-phase currents of the loads, different from PEVs, connected to each one of the lines a, b and c respectively. $I^H_{a_q}$, $I^H_{b_q}$ and $I^H_{c_q}$ are the summation of all the quadrature currents of the loads, different from PEVs, connected to each one of the lines a, b and c respectively.

$$
\begin{aligned}
\mathbf{I}_a = &\left(I^H_{a_d} + \sum_{\forall PEV\ j \in C_a} x_{d_j} \right) \cdot \mathbf{u}_{a_d} \\
&+ \left(I^H_{a_q} + \sum_{\forall PEV\ j \in C_a} x_{q_j} \right) \cdot \mathbf{u}_{a_q} \\
\mathbf{I}_b = &\left(I^H_{b_d} + \sum_{\forall PEV\ j \in C_b} x_{d_j} \right) \cdot \mathbf{u}_{b_d} \\
&+ \left(I^H_{b_q} + \sum_{\forall PEV\ j \in C_b} x_{q_j} \right) \cdot \mathbf{u}_{b_q} \\
\mathbf{I}_c = &\left(I^H_{c_d} + \sum_{\forall PEV\ j \in C_c} x_{d_j} \right) \cdot \mathbf{u}_{c_d} \\
&+ \left(I^H_{c_q} + \sum_{\forall PEV\ j \in C_c} x_{q_j} \right) \cdot \mathbf{u}_{c_q}
\end{aligned}
\tag{6}
$$

Finally replacing equations eq.(6) and eq.(5) in eq.(5) to assess $\mathbf{I}_1$ and $\mathbf{I}_2$, it is possible to define the CUF at a CCP as a function f of the in-phase and quadrature PEV currents as illustrated in eq.(7) supposing that N PEVs are connected.

Equation (7) allow to minimize the CUF by finding and optimal combination of the PEV's in-phase and quadrature currents ($x^*_{d_j}$,$x^*_{q_j}$). These currents are used to assess active and reactive power set-points for each PEV.

$$CUF = f\left(x_{d_1}, x_{d_2}, \ldots, x_{d_N}, x_{q_1}, x_{q_2}, \ldots, x_{q_N}\right) =$$

$$\left(\left(\left(\frac{K_1 + \sum\limits_{\forall PEV\ j \in C_a} x_{d_j} - \frac{1}{2}\left(\sum\limits_{\forall PEV\ j \in C_b} x_{d_j} + \sum\limits_{\forall PEV\ j \in C_c} x_{d_j}\right)}{\left(\left(\left(K_3 + \sum\limits_{\substack{\forall PEV\ j \in C_a \\ \forall PEV\ k \in C_b \\ \forall PEV\ l \in C_c}} x_{d_j} + x_{d_k} + x_{d_l}\right)^2 + \left(K_4 + \sum\limits_{\substack{\forall PEV\ j \in C_a \\ \forall PEV\ k \in C_b \\ \forall PEV\ l \in C_c}} x_{q_j} + x_{q_k} + x_{q_l}\right)^2\right)\right)^{1/2}} + \right.\right.\right.$$

$$\left.\left.\left.\frac{\frac{\sqrt{3}}{2}\left(\sum\limits_{\forall PEV\ j \in C_b} x_{q_j} - \sum\limits_{\forall PEV\ j \in C_c} x_{q_j}\right)}{\left(\left(\left(K_3 + \sum\limits_{\substack{\forall PEV\ j \in C_a \\ \forall PEV\ k \in C_b \\ \forall PEV\ l \in C_c}} x_{d_j} + x_{d_k} + x_{d_l}\right)^2 + \left(K_4 + \sum\limits_{\substack{\forall PEV\ j \in C_a \\ \forall PEV\ k \in C_b \\ \forall PEV\ l \in C_c}} x_{q_j} + x_{q_k} + x_{q_l}\right)^2\right)\right)^{1/2}}\right)^2 + \right.$$

$$\left(\left(\frac{K_2 - \sum\limits_{\forall PEV\ j \in C_a} x_{d_j} + \frac{1}{2}\left(\sum\limits_{\forall PEV\ j \in C_b} x_{q_j} + \sum\limits_{\forall PEV\ j \in C_c} x_{q_j}\right)}{\left(\left(\left(K_3 + \sum\limits_{\substack{\forall PEV\ j \in C_a \\ \forall PEV\ k \in C_b \\ \forall PEV\ l \in C_c}} x_{d_j} + x_{d_k} + x_{d_l}\right)^2 + \left(K_4 + \sum\limits_{\substack{\forall PEV\ j \in C_a \\ \forall PEV\ k \in C_b \\ \forall PEV\ l \in C_c}} x_{q_j} + x_{q_k} + x_{q_l}\right)^2\right)\right)^{1/2}} + \right.\right.$$

$$\left.\left.\left.\frac{\frac{\sqrt{3}}{2}\left(\sum\limits_{\forall PEV\ j \in C_b} x_{d_j} - \sum\limits_{\forall PEV\ j \in C_c} x_{d_j}\right)}{\left(\left(\left(K_3 + \sum\limits_{\substack{\forall PEV\ j \in C_a \\ \forall PEV\ k \in C_b \\ \forall PEV\ l \in C_c}} x_{d_j} + x_{d_k} + x_{d_l}\right)^2 + \left(K_4 + \sum\limits_{\substack{\forall PEV\ j \in C_a \\ \forall PEV\ k \in C_b \\ \forall PEV\ l \in C_c}} x_{q_j} + x_{q_k} + x_{q_l}\right)^2\right)\right)^{1/2}}\right)^2\right)^{1/2} \quad (7)$$

with:

$$K_1 = I_{a_d}^H - \frac{1}{2}\left(I_{b_d}^H + I_{c_d}^H\right) + \frac{\sqrt{3}}{2}\left(I_{b_q}^H - I_{c_q}^H\right) ,$$

$$K_2 = -I_{a_q}^H + \frac{1}{2}\left(I_{b_q}^H + I_{c_q}^H\right) + \frac{\sqrt{3}}{2}\left(I_{b_d}^H - I_{c_d}^H\right) ,$$

$$K_3 = I_{a_d}^H + I_{b_d}^H + I_{c_d}^H ,$$

$$K_4 = I_{a_q}^H + I_{b_q}^H + I_{c_q}^H ,$$

2.2. CUF function validation

In order to validate eq.(7), two scenarios have been performed to compare the CUF assessed with eq.(2) against the CUF assessed using eq.(7) under balanced and unbalanced voltage conditions. In the first scenario, the CCP in Fig.1 is simulated under perfect balanced voltages; therefore on each phase, the voltage phase-to-neutral is equal to 230 V and the phase shift between voltages is equal to 120Â°. In the second scenario, the CCP under voltage unbalance conditions is part of a LV distribution network that connects 18 CCPs gathering 96 householders. The network electrical circuit as well as the transformer and line characteristics are described in Appendix I.

For both scenarios, six residential loads, two per phase, are connected to the CCP. To simulate random loading conditions active and reactive power values are selected randomly from a householders database developed in (Turker, Bacha *et al.*, 2012a). Active power values vary between 0 kW and 9kW while reactive power values vary between -4 kVAr and 4 kVAr. In total, 507 random tests were simulated for each scenario.

Fig.3 shows the CUF assessed for each test using equations eq.(2) and eq.(7). The data is displayed in increasing order. As illustrated, the error between the standard CUF calculation and the one defined by eq.(7) is significantly small.

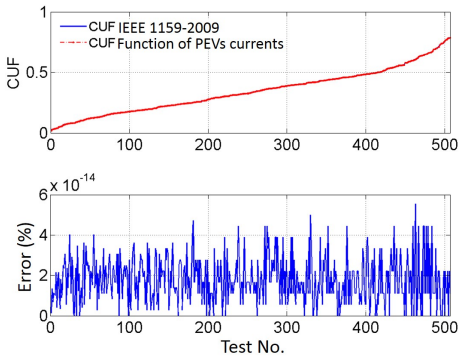

Figure 3. CUF assessment under voltage balanced conditions

Fig.4 shows the VUF assessed at the CCP selected for each one of the tests. The figure confirms that for some tests the VUF exceeds the maximum VUF (2%) allowed for a LV network. Under this voltage unbalanced conditions, the CUF is estimated for each test using eq.(2) and eq.(7) as shown in Fig.5.

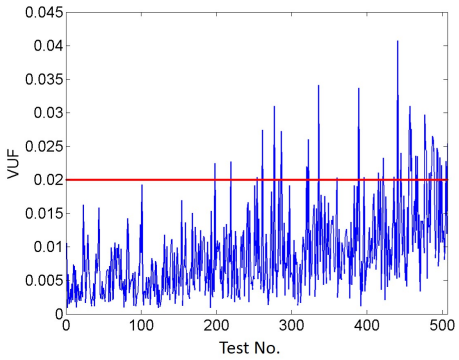

Figure 4. VUF for each test. In red the maximum VUF allowed by the EN 50160

As illustrated by Fig.5, the CUF calculated using eq.(7) differs from the established by IEEE 1159-2009 standard as suggested in the previous section. The maximum error between the approaches is estimated to be around 4%. The error confirmed by the tests is the consequence of assuming constant unitary vectors in order to keep eq.(7). Therefore, eq.(7) diverge from the real CUF with an error when a CCP is under strong voltage unbalance. The CUF minimization under real conditions will be affected by an error on the initial conditions given to the optimization method. As it will be noted in the Results and Discussion section, despite the error, the CUF minimization reduces considerable both the current and the voltage unbalance. A more deeper analysis on the effects of this error on the CUF minimization strategy is beyond the scope of this paper and will be addressed in future studies.

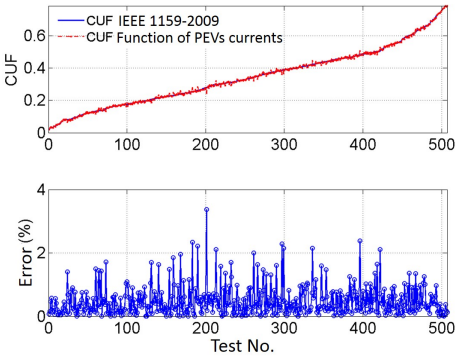

Figure 5. A comparison between the CUF assessed with eq.(2) and the CUF assessed with eq.(7) under voltage unbalance conditions

2.3. PEV Load

As stated by (Nemry *et al*., 2009), several recharging levels for PEVs have been proposed regarding the charging speed and the power driven. Level 1 stands for slow charging, level 2 stands for two semi-fast charging and the level 3 stands for three-phase fast AC and DC charging. In this paper only single phase level 2 charging systems with nominal power of 3 kW are considered. Single-phase charger is chosen in order to address the general impact of single-phase loading on the CUF and consequently, on VUF. CUF minimization using three-phase chargers will be studied in further research.

2.4. Charging interface

The charging interface connects the battery to grid through the charger and the charging station. In the V2G context, PEV interface would have the capability to send energy towards the grid. As stated by (Tuttle, Baldick, 2012), on one side both components of the interface would have to be bidirectional, with maximum power ratings limited by the maximum apparent power of the electric circuit. The charger, on the other side, would have to have the capability of performing power-factor (PF) different than 1 allowing several active and reactive power operation modes. As stated by (Kisacikoglu *et al*., 2013), these operation modes would be capacitive charge, capacitive discharge, inductive charge and inductive discharge. In terms of the PEV charging current and its in-phase and quadrature components (x_{d_j}, x_{q_j} plane), these modes are illustrated by the Fig.6, where the j-th PEV with V2G capability would be able to operate at any current set-point (magnitude and phase regarding the neutral to phase voltage) only limited by the magnitude of the maximum current allowed by the electric circuit ($I_{MAX_{PEV}}$ in Fig.6). For an installation level 2, the $I_{MAX_{PEV}}$ selected is 16 A. Thus, for the CUF minimization, any operation set-point for the j-th PEV must be inside the circular boundary with radius $I_{MAX_{PEV}}$. PEVs limited to only-charging mode are included in the operation region illustrated in Fig.6. Therefore these PEVs can participate in the minimization strategy proposed in this paper without any adjustments. Only bidirectional chargers are considered in this paper in order to take advantage of the future family of PEVs chargers.

2.5. State-of-charge model

The state-of-charge (SOC) model adopted is given by eq.(8) where Q_0 is the nominal capacity of the battery, P_{Batt} is the power at which the battery is charged and ΔT is charging time window of interest.

$$SOC\left(t_k\right) = SOC\left(t_k - \Delta T\right) + \frac{1}{Q_0}\int_0^{\Delta T} P_{Batt}\left(\tau\right)\mathrm{d}\tau$$
$$with\ \Delta T = t_k - t_{k-1} \tag{8}$$

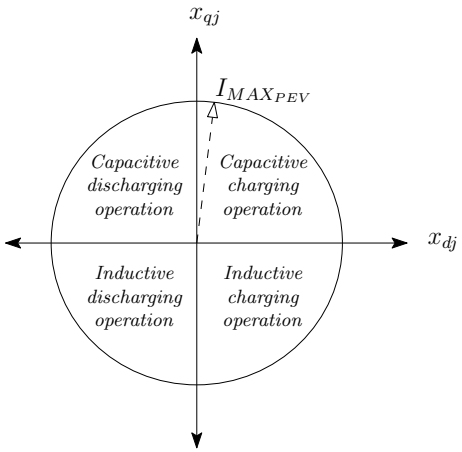

Figure 6. Available currents operation region (x_{d_j},x_{q_j} plane) for the charging electric circuit limited by $I_{MAX_{PEV}}$

Assuming an efficiency of the charger η equal to 0.9 and that the average charging power used from the grid over a period ΔT is P_{Grid}, eq.(8) becomes:

$$SOC\left(t_k\right) = SOC\left(t_{k-1}\right) + \frac{\eta}{Q_0} P_{Grid} \cdot \Delta T \tag{9}$$

The deterioration of the nominal capacity of the battery will not be taken into account in this paper, nevertheless the SOC has to respect the following constraint:

$$30\% < SOC < 100\%$$

3. CUF minimization

The CUF minimization at a CCP is carried out by selecting an optimal set of in-phase and quadrature currents for all the EVs connected to the CCP that minimize the CUF. Each couple x_{d_j},x_{q_j} (j-th EV) has to be below $I_{MAX_{PEV}}$ and the SOC at the departure time has to be enough for EV usage. The optimization problem is stated in eq.(10). The objective function, the constraints and the optimization method are explained in the paragraphs below.

$$
\begin{aligned}
& min_{x \in \Re^{2 \cdot N}} \; f(x) \\
& s.t. \\
& x_{d_j}^2 + x_{q_j}^2 \leq |I_{MAX_{PEV}}|^2 \\
& SOC_{MIN} < P_{Grid_j}(t_k) \cdot \Delta T + SOC_j(t_{k-1}) < SOC_{MAX} \\
& X_{min_{dj}}(t_k) < x_{d_j} \leq |I_{MAX_{PEV}}| \\
& \forall \, j = 1, 2, \ldots, N
\end{aligned}
\tag{10}
$$

3.1. Objective function

The objective function f is the CUF function formulated before in eq.(7). The argument, x, is the set of in-phase and quadrature currents of the N PEVs connected at an instant t_k:

$$x = \left[x_{d_1}, x_{d_2}, \ldots, x_{d_j}, \ldots, x_{d_N}, x_{q_1}, x_{q_2}, \ldots, x_{q_j}, \ldots, x_{q_N}\right]$$

Thus, f is a scalar, convex and non-linear function with input argument in the domain of $\mathbb{R}^{2 \cdot N}$. Active-set algorithm was chosen to optimally solve the optimization problem, a sequential quadratic programming method allowing linear and non-linear constraints (Gill *et al*., 1981).

3.2. Constraints

The first constraint in eq.(10) is related to the maximum ratings allowed by the charging station. In other words, this constraint restrict the values of the in-phase and quadrature currents of the j-th PEV to be inside the circle of radius $||I_{MAX_{PEV}}|$ as illustrated in Fig.6.

The second constraint limits the in-phase current low boundary to variate the charging and discharging rates of the battery (Mohamed *et al*., 2014). This constraint reduce the space of possible in-phase currents values of each PEV in order to ensure maximum SOC at the departure time by avoiding discharges or low charging rates, at a time t_k, if the PEV has a high priority to charge.

3.3. Charging priority constraint

An important part of the real-time CUF minimization strategy is the constraint on the in-phase current depending on the charging priority of the j-th PEV. This priority at a time t_k is defined as high if the PEV does not have enough time to charge the battery, at a minimum charging rate, up to a satisfactory SOC for the daily usage otherwise the priority is low. Enough time is considered as a charging time, T_{charge}^{j}, bigger

than 95% of the remaining time, $T_{remaining}$. The priority is formulated in eq.(11). Charging priority parameter has been chosen as 95% because, after many trials (not shown in this paper) it gives the best compromise between a high CUF minimization and a considerably low amount of PEVs with SOC below 0.9 at the departure time.

$$Priority_j\left(t_k\right) = \begin{cases} High & : T^j_{charge}/T_{remaining} > 0.95 \\ Low & : T^j_{charge}/T_{remaining} \leq 0.95 \end{cases} \tag{11}$$

The charging time, T^j_{charge}, is defined in eq.(12) where SOC_{FINAL} is the desired SOC at the departure time, $SOC\left(t_k\right)$ is the SOC before the depart at the present time t_k, C_0 is the nominal capacity of the battery and $P^{MIN}_{Grid_j}$ is the minimum charging power allowed for operation when the PEV has high charging priority.

$$T^j_{charge} = \left(SOC_{FINAL} - SOC\left(t_k\right)\right)\frac{C_{0_j}}{P^{MIN}_{Grid_j}} \tag{12}$$

Fig.7 illustrates the algorithm to restrict the available currents operation region at t_k based on the priority assessed. According to the algorithm, if the j-th PEV has a high priority to recharge the lower boundary on the in-phase current, $X_{min_{dj}}\left(t_k\right)$, is limited to a minimum charging rate; otherwise if there is not a priority, the minimization solver is allowed to use all the operation plane ($X_{min_{dj}}\left(t_k\right) = -16A$). The minimum charging rate that ensures more than 95% of the times that any PEV is satisfactory charged without significantly affecting the minimization performance, corresponds to $X_{min_{dj}}\left(t_k\right)$ equals to 4 A. This value was empirically assessed. Therefore in eq.(12), $P^{MIN}_{Grid_j}$ is equal to 920 W (4 A * 230 V).

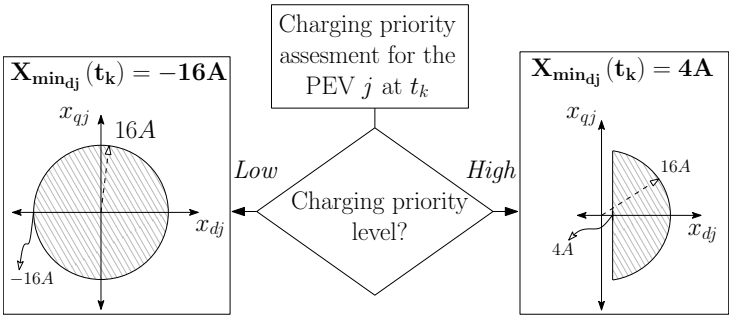

Figure 7. Algorithm to define the currents operation region (x_{d_j},x_{q_j} plane) for the charging installation as a function of the charging priority

4. Real-time CUF minimization strategy

To test the efficiency of the CUF minimization, a Low Voltage Network environment is proposed. To simplify the computational cost, householders and PEVs power

profiles are discretized into a time interval of 10 minutes. Therefore, the CUF (on the 10 minutes basis) is calculated at the time-interval (t_k) with constant values (during the corresponding time-interval) of the currents of the householder and PEVs connected at each CCP. Thus, the CUF at each CCP would be a value refreshed every 10 minutes and the idea of the real-time strategy is to minimize this value at each time interval for each CCP.

Hence, the CUF from the last time-interval is the solver's initial point and the solvers optimal solution, $x^*(t_k)$, would be the in-phase and quadrature optimal currents of each PEV for the present time-interval. Moreover, at every time interval, the dimension of the objective function changes due, firstly to disconnection or connection of PEVs and secondly to the change on the householders consumption. Thus, another reason of a real-time strategy is to adapt the optimization problem to the changing nature of the parameters. The Real-time CUF minimization (RTCM) strategy is illustrated in the Fig.8.

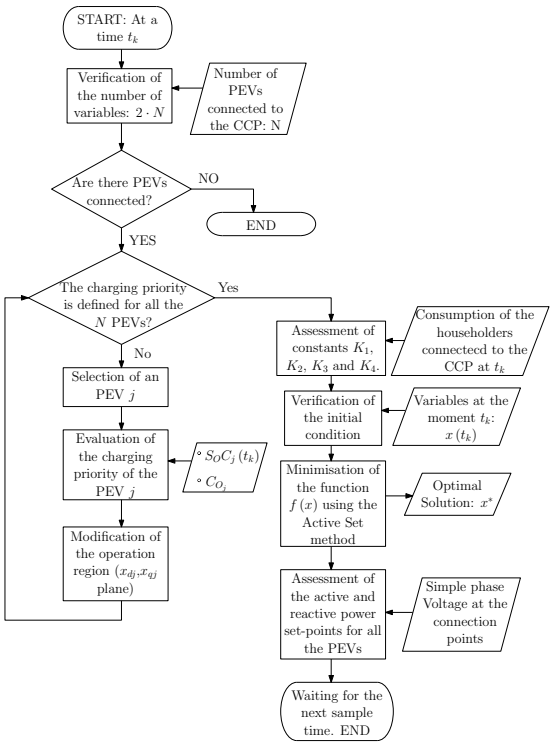

Figure 8. Flow diagram describing the Real-time minimization strategy

The strategy follows several stages:

1. It starts at the time interval t_k

2. The number N of PEVs connected to a CCP is verified in order to establish the number of variables available for the CUF minimization. The number of variables is

two times N because each PEV contribute with two control variable. If there is no PEVs connected to the CCP the algorithm stops.

3. Once the number of variables is determined, the charging priority is evaluated for each PEV as explained on the previous section:

a) To evaluate the charging priority, each PEV should provide information on the SOC at t_k and its maximum capacity, C_{0_j}.

b) The operation region is modified based on the charging priority, ensuring maximum charge for each PEV at the departure time.

4. After defining the charging priority for all the PEVs, constants K_1, K_2, K_3 and K_4 are assessed using information available on the consumption of the householders connected to the CCP at t_k.

5. The set of currents of the PEVs at $t_k - 1$, $x\left(t_k - 1\right)$, is verified in order to establish the initial condition

6. Active-set algorithm is launched over the conditions established by the previous stages. The set of in-phase and quadrature currents, x^*, that minimize the CUF at the time interval t_k is the optimal solution.

7. The active and reactive powers set-points for each PEV are assessed using x^* and the simple phase voltages at the connection points .

8. Finally the minimization system enters in stand by mode until the next sample time.

To test this strategy, a simulation environment is proposed in the next section.

5. Simulation of a low voltage network

The simulation scenario is composed by a LV electric network connecting an MV/LV Transformer to householder and PEV loads. The simulation scenario covers a window of time of one week with a time step of 10 minutes.

The electric network simulated is a low-voltage network composed by 96 houses grouped in 18 CCPs connected to the MV network through a 400 kVA transformer. The network's electrical circuit as well as the transformer and the line characteristics are presented in Appendix I.

The simulation process is illustrated by the scheme in Fig.9. The simulation starts by setting the initial time conditions (Day 0 and minute 0). Then, the number of PEVs per householder is chosen randomly as well as the battery capacity for each one of them.

The simulation of the week is run day by day. In the initialization stage (for each day) the arrival and the departure time, the initial State-of-Charge (SOC_0) as well as the householder's daily load profile are chosen randomly based on the characteristics described in the previous section. The charging power at the arrival time is set to 3 kW.

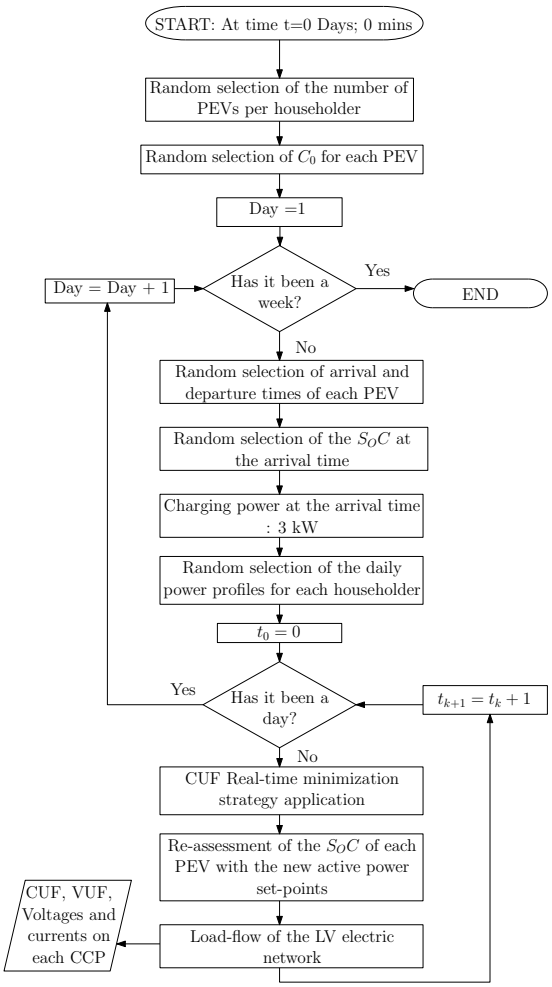

Figure 9. Flow diagram describing the simulation process

Once the daily initial conditions are set, the simulation of the day is executed on 10 minutes time basis. At every time interval, the RTCM strategy is applied to minimize the CUF under the present time step conditions. Then, the optimal active power set-points are used to re-assess the SOC of the battery of each PEV. After that, the load-flow on the electric network is executed in order to calculate the voltages and currents, as well as, the CUF and the VUF data. Finally, after completing a day, the process is repeated day by day, until a week is simulated. In the following paragraphs, the stochastic characteristics of householder's and PEV's profiles are described.

5.1. Householders power profiles

The weekly consumption for each householder is randomly selected from a database developed in (Turker, Bacha *et al*., 2012a) composed by over 2000 summer power profiles. The active power varies between 0 kW and 9 kW while the reactive power varies between 0 kVAr and 4 kVAr. Each weekly profile is composed by 1050 samples each representing a 10 minutes duration. The values of the active and reactive powers during each interval of time represents the average of the active and reactive powers consumed by the load.

5.2. PEV power profiles parameters

The main characteristics of the PEV power profiles are the random number of PEVs connected, the random connection times, the random disconnection times, the random battery capacities, the charging power limited by the electric circuit and the random SOC at the arrival time.

The number of PEVs per house holder has been chosen randomly following the method proposed in (Duvall *et al*., 2011). The probability density function (PDF) for the random selection takes into account the statistics of vehicles per householders in a specific social scenario and the combinatorial PDF describing the probability that a vehicle is a PEV as a function of the market penetration ratio. For the simulation 107 PEVs were distributed among the 96 householders following the statistics of number of vehicles per house holder in France (Turker, Bacha *et al*., 2012b) and a market penetration ratio of 100 % of PEVs. This market penetration level is a futuristic scenario, in which all citizens with vehicles have PEVs exclusively. A lower market penetration level will imply both less impact of the PEV fleet on the CUF and the VUF and, on the other hand, a smaller capability of improving the CUF at the distribution network.

The random selection of the connection and the disconnection times is based on the PDFs presented in (Duvall *et al*., 2011) and in (Turker, Hably *et al*., 2012) respectively. The PDF for the connection times assumes that the PEVs are connected intermediately after they arrive to their residences, and the most probable arrival times (more than 60% of them) are between 5 PM and 8 PM. In addition, the disconnection time is identified as the time of the day where users are most probably (more than 70% of the times) leaving their places. Approximately 70% of the PEV users leave their residences between 5 AM and 8 AM.

For the random selection of the batteries capacities, C_0, a random selection was implemented for each one of the PEVs with a PDF based on the classification done in (Turker, Bacha *et al*., 2012a). This classification takes into account the size of the PEV and the all-electric-range (AER) of 3 types of PEVs (Including PHEVs). The battery sizes vary between 5 kWh and 27 kWh.

For the charging power this will be determined by the real-time strategy and consequently it will be limited by the electric circuit of a level 2 simple phase installation as explained in section II.

Finally the SOC at the arrival time, SOC_0, would be selected for each PEV every day of the week simulated, by a random selection based of 3 probable options: 70% of the PEVs are expected to arrive with an SOC between 0.3 and 0.49; 20% of the PEVs are expected to arrive with an SOC between 0.5 and 0.79 and 10% of the PEVs are expected to arrive with an SOC between 0.8 and 1.

The influence of the parameters such as the market penetration ratio, the SOC_0, C_0, the arrival, departure and disconnection times as well as their probability density function parameters will be subject of future research.

6. Results and discussion

In total 1050 samples of each, CUF and VUF, were collected for each CCP, in other words, 145 per day (10 minutes basis). Fig.10 and Fig.11 show CUF and VUF profiles during a day of the data collected on the CCP No.9 for several scenarios. In the first scenario, the LV network connects only householders. In the second scenario, the LV network connects householders and PEVs but there is no RTCM strategy controlling the PEVs connected. In the third scenario, the LV network connects householders and PEVs and the RTCM strategy controls the PEV charge.

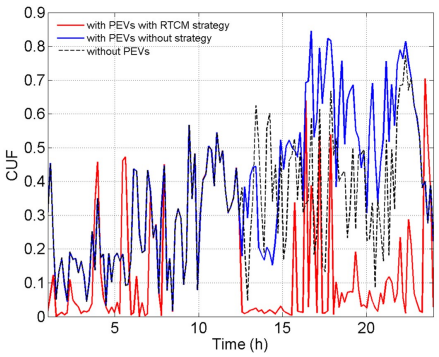

Figure 10. Daily CUF profile of the CPP number 9 connected to the LV electric network: scenario 1) without PEVs; scenario 2) with PEVs without strategy; scenario 3) with PEVs with the RT minimization strategy

Regarding the CUF profile on Fig. 10, it is possible to notice that the introduction of the PEVs increases the CUF for the most of the time intervals. Moreover, in most of the intervals, the RTCM strategy reduces the CUF, even below the CUF from the scenario with no PEVs connected. Nevertheless, there are some intervals where the strategy causes greater CUF than that one of the other scenarios. The reason for this is that in the third scenario the charging priority constraint limits the space of solutions, therefore optimal solutions that coincide with the no strategy scenarios might not be reachable.

On Fig.11, the red dot-dash line illustrates the maximum value of VUF a CCP is allowed to have according to the standard EN50160. The figure shows that the con-

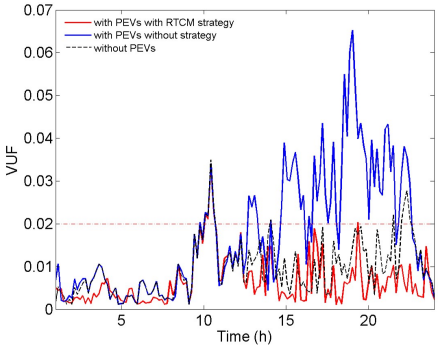

Figure 11. Daily VUF profile of the CPP number 9 connected of the LV electric network. The three scenarios are illustrated

nection of the PEVs cause significant unbalance more noticeable at peak consumption hours. It also shows how the implementation of the RTCM strategy improves the VUF mesured at a CCP, in this case the CCP No. 9. In the Fig.11, the effect of the algorithm is more noticeable during the evening when most of the PEVs would be more likely connected to the CCP.

6.1. CUF Analysis

The Fig.12 illustrates the data collected on the CUF for the third scenario. Each color represents one of the CCPs. The limit drawn by the black dashed line ($CUF = 0.1$) is used to define a current balance index, CBI. The CBI is the percentage of the data below 0.1 taken into account all the CPPs of the network studied (Electrical, departement, 2005). The CBI for the three scenarios is presented in Table 1.

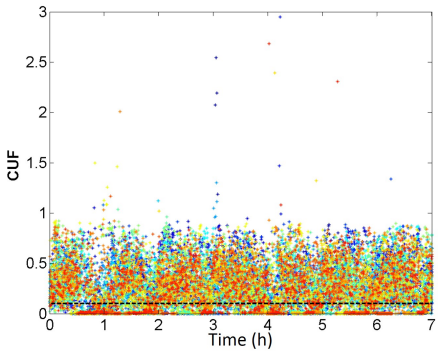

Figure 12. Weekly CUF profile for the third scenario. Each color represents a CCP connected to the LV network.

Comparing the CBI in Table 1 for each scenario, the RTCM strategy improves the index by more than 20 points (absolute difference). Regarding the relative difference,

Table 1. Current balance Index (CBI) for the three scenarios studied

Scenario	without PEVs	PEVs without strategy	PEVs with RTCM strategy
CBI (%)	5.96	5.39	47.28

the CBI achieved in the third scenario is more than 4 times the CBI obtained in the first and second scenarios. In other words, the number of CUF samples below 0.1 increases four times by using the RTCM strategy.

6.2. VUF Analysis

Several network parameters affect the voltage unbalance at each CCP (Jayatunga *et al*., 2012): the distance between the feeder and the CCP, the CUF generated by the loads connected to the CCP and the voltage unbalance generated by other CCPs. For this reason, firstly the impact of the RTCM strategy on the VUF is analyzed on a specific CCP, in this case the CCP chosen is the No. 9.

The VUF samples over the week on the CCP No. 9, are illustrated in the Fig.13. To compare the different scenarios, a voltage unbalance index, VUI, is used. The VUI is the percentage of the data below 0.02 (the black dashed line in the illustration). Thus a CCP is balanced if the VUI is over 95% according to the definition of the standard EN 50160. The VUI for the three scenarios is presented in Table 2.

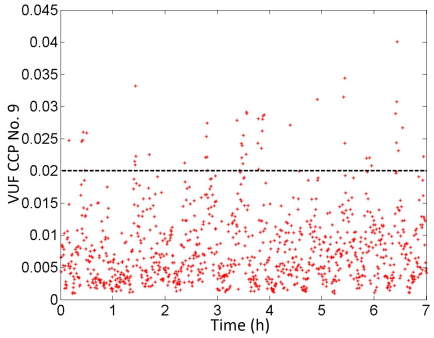

Figure 13. Weekly VUF profile for the CCP No. 9 collected from the third scenario

Table 2. Voltage Unbalance Index (VUI) for the three scenarios studied

Scenario	without PEVs	PEVs without strategy	PEVs with RTCM strategy
VUI (%)	92.22	77.63	96.06

According to the VUI in Table 2 for each scenario, the RTCM strategy improves the VUI by more than 17 points (absolute difference) regarding the second scenario and by approximately 3 points regarding the first scenario. In other words, the number of VUF samples below 0.02 increases by using the RTCM strategy. More importantly, the CCP No.9 , unbalanced in the scenario without PEVs, has been balanced thanks to the action of the PEVs connected and controlled by the RTCM strategy.

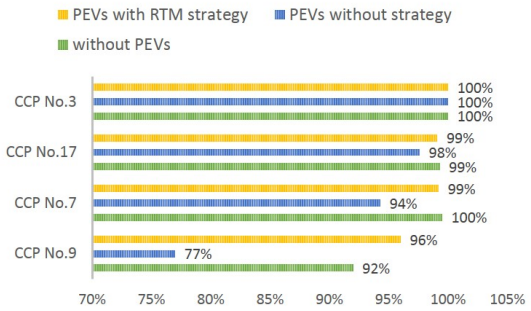

Figure 14. VUI at CPP No. 9, No. 7, No. 17 and No. 3 for the three scenarios considered

In order to illustrate the dependance of the RTCM on the CCP characteristics for each one of the scenarios, the VUI is assessed for 3 different CCPs. Fig.14 presents the VUI values per scenario measured on the CCP No.9, No.7, No.17 and No.3. As shown on the figure, the VUI at the CPP No. 9 represents the worst case scenario among the CCPs. In addition, for some of the CPPs, like the No. 3, the VUI is not deteriorated by the introduction of the PEVs. On the other hand, the VUI is improved by the RTCM strategy for the CCPs No. 7 and No. 17, being the higher improvement on the CCP No. 9. A detailed analysis of the VUI as a function of the characteristics of the system goes out of the scope of this paper.

6.3. Charging constraints analysis

To evaluate how well the RTCM strategy preserves a high SOC at the departure time, the third scenario has been simulated firstly without the charging priority constraint and, secondly taking it into account. To compare both situations, a satisfactory SOC has been supposed to be bigger than 0.9. Therefore, if a PEV has a SOC less than 0.9 at its departure time, this PEV is said to have unfulfilled its energy needs for the day.

Fig.15 presents the frequency density of the SOC samples at the departure time for the scenario using the RTCM strategy taking into account the charging priority constraint. Each red bar in the figure represents the percentage of data per classification interval. It can be seen that approximately 80 % of the SOC samples are located between 1 and 0.98 and approximately 3.69 % are below 0.9 (inside the doted square).

In other words, in less than 4% of the departure events, the PEVs had an unsatisfactory SOC.

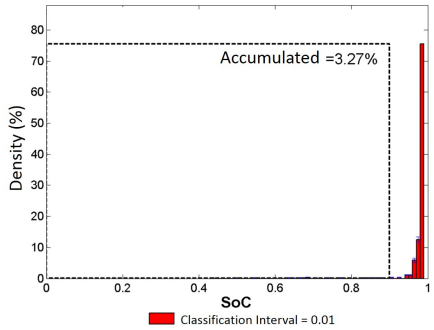

Figure 15. Frequency density of the SOC samples at the departure time. PEVs take part of the RTCM strategy with the charging priority constraint

Fig.16 presents the frequency density of the SOC samples at the departure time for the scenario using the RTCM strategy without the charging priority constraint. Approximately in 27% of the departure events the SOC is below 0.9. In other words, in more than 27% of the departure events, the PEVs had an unsatisfactory SOC.

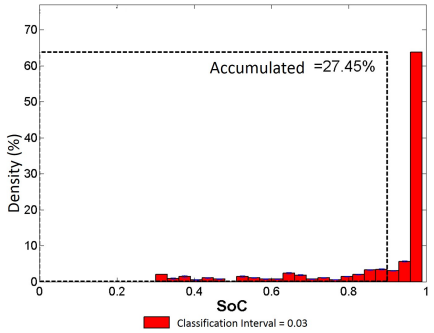

Figure 16. Frequency density of the SOC samples at the departure time. PEVs take part of the RTCM strategy wihtout the charging priority constraint

Table 3 summarizes the percentage of unsatisfactory departure events for three different simulation conditions: First the PEVs charge without strategy, second the PEVs participate in the strategy taking into account the charging priority constraint and third the PEVs participate in the strategy without the charging priority constraint. As the percentages show, the constraint reduces unsatisfactory depart events at almost the same level of the scenario of the PEVs charging without strategy.

Table 3. Percentage of unsatisfactory departure events for different simulation conditions

Simulation conditions	without strategy	strategy with charging constraint	strategy without charging constraint
Events (%)	2.91	3.27	27.45

6.4. Active and reactive power set-points

Fig.17 illustrates the frequency density of active (P) and reactive (Q) power set-points given the RTCM strategy. Over 15.205 of set-point samples are located on a [P,Q] plane where the maximum charging power constraint ($16A{\cdot}230V$) is represented by the doted circumference. From this representation it is possible to conclude firstly that active-power production set-points are less frequent than active-power consumption set-points. This characteristic is a consequence of the charging priority constraint that is located on the figure by the high density vertical line. The remaining set-points are distributed rather homogeneously.

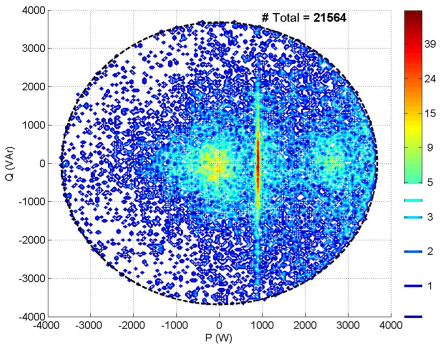

Figure 17. Frequency density of active and reactive power set-points . Towards the red high set-points density. Classification surface := 50 W x 50 VAr

7. Conclusions and future work

A real-time current unbalance factor minimization strategy has been proposed. Current unbalance factor measured at a common connection point has been modeled as a function of the local PEV in-phase and quadrature currents. This model in addition to maximum ratings and charging priority constraints have been used to formulate a minimization problem. Then a real-time minimization strategy has been proposed to

adapt the optimization problem every time step to the changing number of PEVs connected and householder consumption. Furthermore a simulation case study has been proposed to test the strategy for CCP with different characteristics. The positive impact of the strategy on the current and voltage unbalance factors was studied and it has been shown through data analysis that an improvement on the unbalance conditions is attainable by the RTCM strategy.

As further work, several challenges should be addressed. The voltage unbalance effects on the CUF assessment have to be included in the objective function in order to improve the minimization outcome. Additionally, the voltage unbalance factor has to be characterized in terms of CCP and grid characteristics. This would allow to formulated an optimization problem for the voltage unbalance. In addition, a sensitivity analysis on the simulation parameters must be considered, given that this parameters will vary considerable depending on the social and technological context of the distribution network chosen. Furthermore, Three-phase chargers should be considered in the optimization problem taking into account the growing number of three-phase charging stations installed among PEV residential owners. Moreover, the profit for both actors, PEV owners and the grid has to be assessed in order to quantify the benefit of this new V2G service. Finally, the positive impact of CUF minimization on the sustainability of the power system (Distribution Network) should be assessed. This Assessment could open new research opportunities on the participation of PEVs and end-users in the improvement of the power quality.

References

Duvall M., Alexander M., Maitra A., Saucedo D., Jungers B., Halliwell J. *et al.* (2011). *Transportation electrification: a technology overview.*

Electrical E., departement G. o. H. K. mechanical service. (2005). *Code of practice for energy efficiency of electrical installations*. Technical report. Electrical and mechanical service departement.

Fernandez J., Bacha S., Riu D., Hably A. (2015, March). Plug-in electric vehicle collaborative charging for current unbalance minimization: Ant system optimization application. In *Industrial technology (icit), 2015 ieee international conference on*, p. 2686-2691.

Fernandez J., Bacha S., Riu D., Turker H., Paupert M. (2013, Feb). Current unbalance reduction in three-phase systems using single phase phev chargers. In *Industrial technology (icit), 2013 ieee international conference on*, p. 1940-1945.

Fernandez J., Hably A., Bratcu A. (2015, March). Assessing the economic profit of a vehicle-to-grid strategy for current unbalance minimization. In *Industrial technology (icit), 2015 ieee international conference on*, p. 2628-2635.

Francfort J. (2013, March). *U.s. department of energys vehicle technologies program*. Technical report. Idaho National Laboratory Publications.

Gill P. E., Murray W., Wright M. H. (1981). *Practical optimization*. London, Academic Press.

Gomez J., Morcos M. (2003, July). Impact of ev battery chargers on the power quality of distribution systems. *Power Delivery, IEEE Transactions on*, Vol. 18, No. 3, pp. 975-981.

Hu W., Su C., Chen Z., Bak-Jensen B. (2013, July). Optimal operation of plug-in electric vehicles in power systems with high wind power penetrations. *Sustainable Energy, IEEE Transactions on*, Vol. 4, No. 3, pp. 577-585.

Ieee recommended practice for monitoring electric power quality. (2009, June). *IEEE Std 1159-2009 (Revision of IEEE Std 1159-1995)*, pp. c1-81.

Jayatunga U., Perera S., Ciufo P. (2012, July). Voltage unbalance emission assessment in radial power systems. *Power Delivery, IEEE Transactions on*, Vol. 27, No. 3, pp. 1653-1661.

Kempton W., Letendre S. E. (1997). Electric vehicles as a new power source for electric utilities. *Transportation Research Part D: Transport and Environment*, Vol. 2, No. 3, pp. 157–175.

Kisacikoglu M., Ozpineci B., Tolbert L. (2013, Dec). Ev/phev bidirectional charger assessment for v2g reactive power operation. *Power Electronics, IEEE Transactions on*, Vol. 28, No. 12, pp. 5717-5727.

Lassila J., Tikka V., Haakana J., Partanen J. (2012, December). Electric cars as part of electricity distribution - who pays, who benefits ? *Electrical Systems in Transportation, IET*, Vol. 2, No. 4, pp. 186-194.

Markiewicz H., Klajn A. (2004). Voltage disturbances–standard en 50160. *Copper Development Association, lEE Endorsed Provider, Wroclaw University of Technology*.

Mohamed A., Salehi V., Ma T., Mohammed O. (2014, April). Real-time energy management algorithm for plug-in hybrid electric vehicle charging parks involving sustainable energy. *Sustainable Energy, IEEE Transactions on*, Vol. 5, No. 2, pp. 577-586.

Nemry F., Leduc G., Munoz A. (2009). *Plug-in hybrid and battery-electric vehicles: State of the research and development and comparative analysis of energy and cost efficiency*. Technical report. Institute for Prospective and Technological Studies, Joint Research Centre.

Shahnia F., Ghosh A., Ledwich G., Zare F. (2012, July). An approach for current balancing in distribution networks with rooftop pvs. In *Power and energy society general meeting, 2012 ieee*, p. 1-6.

Shahnia F., Ghosh A., Ledwich G., Zare F. (2013). Predicting voltage unbalance impacts of plug-in electric vehicles penetration in residential low-voltage distribution networks. *Electric Power Components and Systems*, Vol. 41, No. 16, pp. 1594-1616.

Shahnia F., Wolfs P., Ghosh A. (2013, July). Voltage unbalance reduction in low voltage feeders by dynamic switching of residential customers among three phases. In *Power and energy society general meeting (pes), 2013 ieee*, p. 1-5.

Sortomme E., El-Sharkawi M. (2012, March). Optimal scheduling of vehicle-to-grid energy and ancillary services. *Smart Grid, IEEE Transactions on*, Vol. 3, No. 1, pp. 351-359.

Turker H., Bacha S., Chatroux D., Hably A. (2012a, July). Low-voltage transformer loss-of-life assessments for a high penetration of plug-in hybrid electric vehicles (phevs). *Power Delivery, IEEE Transactions on*, Vol. 27, No. 3, pp. 1323-1331.

Turker H., Bacha S., Chatroux D., Hably A. (2012b). Modelling of system components for vehicle-to-grid (v2g) and vehicle-to-home (v2h) applications with plug-in hybrid electric vehicles phevs. In *Isgt*, pp. 1–8.

Turker H., Hably A., Bacha S., Chatroux D. (2012, Jan). Rule based algorithm for plug-in hybrid electric vehicles (phevs) integration in residential electric grid areas. In *Innovative smart grid technologies (isgt), 2012 ieee pes*, p. 1-7.

Tuttle D., Baldick R. (2012, March). The evolution of plug-in electric vehicle-grid interactions. *Smart Grid, IEEE Transactions on*, Vol. 3, No. 1, pp. 500-505.

Wang Z., Wang S. (2013, July). Grid power peak shaving and valley filling using vehicle-to-grid systems. *Power Delivery, IEEE Transactions on*, Vol. 28, No. 3, pp. 1822-1829.

Appendix

LV network

The electrical circuit of the LV network used for simulation is presented in Fig.18.

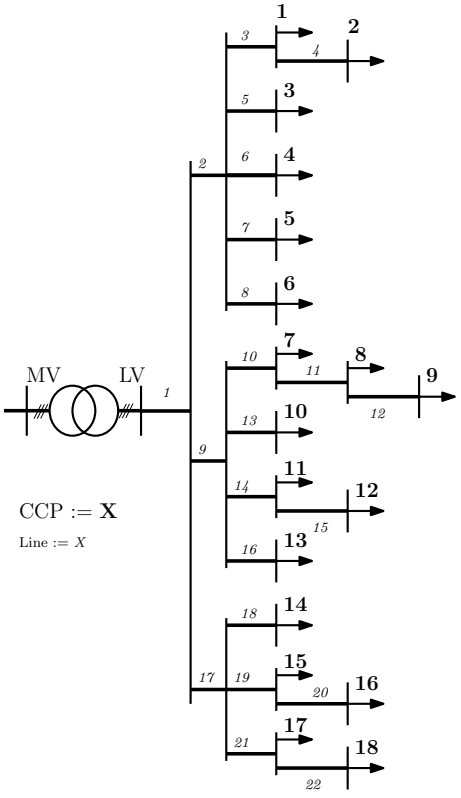

Figure 18. Network's electrical circuit

Table 4, lists the parameters of the MV/LV transformer model used for the simulations in this paper. In the Table 5, the line parameters of the LV network used for the simulations in this paper are presented. The conductor used is an underground aluminum type 3.

Table 4. MV/LV transformer parameters

Full-load power	400 kVA
Rated voltage on MV side	20 kV
Rated voltage on LV side	400 V
No-load losses	930 W
Full-load losses	4600 kW
Short-circuit voltage	4%
No-load current	1.9%
Voltage droop at $\cos(\phi) = 1$	1.22%
Voltage droop at $\cos(\phi) = 0.8$	3.25%
Efficiency at $\cos(\phi) = 1$	98.64%
Efficiency at $\cos(\phi) = 0.8$	98.3%
Resistance (from LV side)	4.88 $m\Omega$
Reactance (from LV side)	15.53 $m\Omega$
Iron losses equiv. resistance	143.37 $m\Omega$
MV side rotary inductance	167.53 mH
Full-load MV side current	11.55 A
Full-load LV side current	577.35 A

Table 5. Line parameters of the LV network

Line	Cross-sectional area (mm^2)	Neutral cross-sectional area (mm^2)	Length (m)	Cap. ($\mu\frac{F}{m}$)	Imp. (Ω/km)
1	240	95	78	0.27	$0.125 + i * 0.75$
2	240	95	33	0.27	$0.125 + i * 0.75$
3	150	70	408	0.225	$0.206 + i * 0.76$
4	70	50	523	0.186	$0.443 + i * 0.78$
5	95	50	382	0.19	$0.32 + i * 0.77$
6	70	50	309	0.186	$0.443 + i * 0.78$
7	150	70	158	0.225	$0.206 + i * 0.76$
8	95	50	274	0.19	$0.32 + i * 0.77$
9	240	95	52	0.27	$0.125 + i * 0.75$
10	150	70	751	0.225	$0.206 + i * 0.76$
11	95	50	244	0.19	$0.32 + i * 0.77$
12	70	50	414	0.186	$0.443 + i * 0.78$
13	95	50	342	0.19	$0.32 + i * 0.77$
14	95	50	124	0.19	$0.32 + i * 0.77$
15	95	50	238	0.19	$0.32 + i * 0.77$
16	70	50	625	0.186	$0.443 + i * 0.78$
17	240	95	68	0.27	$0.125 + i * 0.75$
18	150	70	552	0.225	$0.206 + i * 0.76$
19	150	70	228	0.225	$0.206 + i * 0.76$
20	95	50	354	0.19	$0.32 + i * 0.77$
21	95	50	595	0.19	$0.32 + i * 0.77$
22	70	50	312	0.186	$0.443 + i * 0.78$